J. Biochem. **130**, 107–118 (2001)

X-Ray Crystalline Structures of Pyrrolidone Carboxyl Peptidase from a Hyperthermophile, *Pyrococcus furiosus*, and Its Cys-Free Mutant

Hideaki Tanaka,* Masanobu Chinami,† Tsunehiro Mizushima,* Kyoko Ogasahara,* Motonori Ota,‡ Tomitake Tsukihara,* and Katsuhide Yutani*,[1]

**Institute for Protein Research, Osaka University, 3-2 Yamadaoka, Suita, Osaka, 565-0871; †Department of Nutritional Science, Kyushu Women's University, 1-1 Jiyugaoka, Yahatanishi, Kitakyushu, Fukuoka, 807-8086; and ‡National Institute of Genetics, Yata Mishima, Shizuoka 411-8540*

Received March 12, 2001; accepted April 20, 2001

In order to elucidate the mechanism of the thermostability of proteins from hyperthermophiles, X-ray crystalline structures of pyrrolidone carboxyl peptidase from a hyperthermophile, *Pyrococcus furiosus* (*Pf*PCP), and its mutant protein with Ser substituted at Cys142 and Cys188 were determined at 2.2 and 2.7 Å resolution, respectively. The obtained structures were compared with those previously reported for pyrrolidone carboxyl peptidases from a hyperthermophilie, *Thermococcus litoralis* (*Tl*PCP), and from a mesophile, *Bacillus amyloliquefaciens* (*Ba*PCP). The *Pf*PCP structure is a tetramer of four identical subunits similar to that of the *Tl*PCP and *Ba*PCP. The largest structural changes among the three PCPs were detected in the C-terminal protrusion, which interacts with that of another subunit. A comparison of the three structures indicated that the high stability of *Pf*PCP is caused by increases in hydrophobic interactions and hydrogen bonds, the formation of an intersubunit ion-pair network, and improvement to an ideal conformation. On the basis of the structures of the three proteins, it can be concluded that *Pf*PCP does not have any special factors responsible for its extremely high stability and that the conformational structure of *Pf*PCP is superior in its combination of positive and negative stabilizing factors compared with *Ba*PCP.

Key words: hyperthermophile, *Pyrococcus furiosus*, pyrrolidone carboxyl peptidase, thermal stability, X-ray structure.

The conformations of general globular proteins from mesophiles are marginally maintained by a combination of many positive (such as hydrogen bonds and hydrophobic interaction) and negative (such as entropic factors and steric hindrance) factors for stabilization (*1*). Studies on extremely thermostable proteins from hyperthemophiles that have denaturation temperatures above 100°C would be expected to help in understanding the stabilization mechanism of general globule proteins. Recently, the X-ray structures of many proteins from hyperthermophiles have been determined and several factors responsible for extremely thermostable proteins have been proposed, including an increase in the number of ion-pairs and hydrogen bonds (*2–11*), an increase in core hydrophobicity (*12*, *13*), decreases in the length of surface loops and peptide chains (*11*, *14*), increases in packing density (*14*, *15*), and the oligomerization of several subunits (*16–21*). However, the origin of extremely high thermostability at the molecular level has not yet been determined. This might be because the stability results in a combination of many factors and the contribution of each factor to thermostability cannot yet be estimated quantitatively.

The pyrrolidone carboxyl peptidase [EC 3.4.19.3] (*Pf*PCP) from a hyperthermophilic archaeon, *Pyrococcus furiosus*, which removes amino-terminal L-pyroglutamic acid from peptides and proteins, is a suitable protein for the physicochemical exploration of the stabilization mechanism of hyperthermophile proteins, because the thermal denaturation of *Pf*PCP is completely reversible under some conditions and can be thermodynamically analyzed (*22*, *23*). In the case of hyperthermophile proteins, the thermal denaturation is generally irreversible and only a few small proteins are reported to be reversibly denatured (*24*, *25*). In order to elucidate the mechanism of the thermal stability of *Pf*PCP, its three-dimensional structure is needed. Thus we have analyzed the X-ray structure of this protein.

Recently, the X-ray structures of pyrrolidone carboxyl peptidase (*Tl*PCP) from the hyperthermophilic archaeon, *Thermococcus litoralis* (*26*), and (*Ba*PCP) from a mesophile, *Bacillus amyloliquefaciens* (*27*), have been reported. From the *Tl*PCP structure, the highly hydrophobic insertion that forms the core of the PCP tetramer and the presence of intersubunit disulphide bonds between Cys190 residues in each subunit seem to be responsible for the stability (*26*). The Cys190 in *Tl*PCP corresponds to Cys188 in *Pf*PCP, but there is no corresponding Cys in *Ba*PCP. Cys188 in *Pf*PCP hardly forms a disulphide bond in solution, but the stability increases remarkably when Cys188 is oxidized (*23*). This

[1] To whom correspondence should be addressed. Phone: +81-6-6879-8615, Fax: +81-6-6879-8616, E-mail: yutani@protein.osaka-u.ac.jp

Abbreviations: *Pf*PCP, *Tl*PCP, and *Ba*PCP are pyrrolidone carboxyl peptidase from *Pyrococcus furiosus*, *Thermococcus litoralis*, and *Bacillus amyloliquefaciens*, respectively; *Pf*C142/188S, Cys-free mutant *Pf*PCP (Cys142→Ser and Cys188→Ser); DSC, differential scanning calorimetry; NCS, non-crystallographic symmetry; SPMP, stability profiles of mutant proteins.

has been confirmed by DSC (Differential Scanning Calorimetry) experiments using a Cys-free mutant *Pf*PCP (*Pf*C142/188S) (*23*). The Cys-free mutant is very suitable for calorimetry because Cys residues introduce complexity into the heat capacity curve in DSC.

Therefore, in this study, we determined the X-ray structures of *Pf*PCP at 2.2 Å resolution and its Cys-free mutant protein (*Pf*C142/188S) at 2.7 Å. The origin of the extremely high stability of proteins from hyperthermophiles will be discussed on the basis of the structures of the newly determined *Pf*PCPs, and those already reported for *Tt*PCP and *Pf*PCP.

MATERIALS AND METHODS

Purification and Crystallization of PfPCP—The wild type PCP (*Pf*PCP) from *P. furiosus* was expressed in *Escherichia coli* strain JM109/pPCP3. The Cys mutant protein of *Pf*PCP with Ser substituted at positions Cys142 and Cys188 (*Pf*C142/188S), was constructed by site-directed mutagenesis (*22*). *Pf*PCP and *Pf*C142/188S were purified as described previously (*22*). Crystallization experiments were carried out at 25°C using the hanging-drop vapor diffusion method. The concentrations of both purified proteins were adjusted to 10 mg/ml in 80 mM Na-acetate buffer, pH 4.6 [including 4 mM EDTA and 4 mM dithioerythritol (DTE) in the case of the *Pf*PCP]. Crystals of *Pf*PCP were obtained from a reservoir solution containing 80 mM Na-acetate buffer, pH 4.6, including 4 mM EDTA and 4 mM DTE and 4% (w/v) PEG 4 K. Crystals of the *Pf*C142/188S mutant were obtained from a reservoir solution containing 80 mM Na-acetate, pH 4.6, 0.5 M ammonium sulfate and 30% (v/v) 2-methyl-2,4-pentanediol (MPD). Both crystals, the wild type and its Cys mutant, belong to space group $P2_1$ with cell dimensions of a = 57.9 Å, b = 105.0 Å, c = 78.5 Å, and β = 90.7°, and a = 49.0 Å, b = 105.8 Å, c = 105.8 Å, and β = 96.2°, respectively.

X-Ray Data Collection—The X-ray intensity data for *Pf*PCP were collected on Rigaku R-AXIS IIC imaging plates using graphite-monochromated CuKα radiation. The data for *Pf*C142/188S were measured in Mac Science DIP2030 nickel-filtered double-mirror focused CuKα-radiation. A Rigaku RU-200 rotating-anode X-ray generator was operated at 40 kV and 100 mA. Crystals of wild-type and mutant PCPs diffracted up to 2.2 and 2.5 Å resolution, respectively. The intensity data were processed and integrated by the program DENZO and scaled by the program SCALEPACK (*28*). Data collection statistics are summarized in Table I.

Structure Determination and Refinement—The structure of *Pf*PCP was solved by the molecular replacement (MR) method using the X-PLOR package with the X-ray structure of PCP from *Bacillus amyloliquefaciens* (*Ba*PCP, PDB entry No. 1AUG). The initial sigma-a weighted electron density map was then refined by solvent flattening (*29*), histogram mapping (*30*), and the non-crystallographic symmetry (NCS) averaging technique (*31*, *32*) using the program DM from the CCP4 suite (*33*). The modified electron density map showed the main chain and most of the side chains. PCP was a homotetramer of four independent monomers related by noncrystallographic 222 symmetry. One molecule was built into the electron density map using the program TURBO-FRODO version 5.5 (*34*), and other molecules in the asymmetric unit were generated by the NCS operation. Because the electron density of the N-terminal and C-terminal loop was not clear, $2F_o$–F_c omit maps were used to built structural models of these regions. Simulated annealing, positional and B-factor refinement were carried out using the diffraction data in the resolution range between 10 to 2.2 Å with the program X-PLOR (*35*). The crystal structure was restrained under NCS operations during the refinements. The final round of B-factor refinement used the program CNS (*36*) by including bulk-solvent scaling (*37*). The structure of the mutant protein, *Pf*C142/188S, was determined by the MR technique using the obtained tetrameric model of *Pf*PCP. Structure refinement of the mutant PCP was performed by following that of the wild-type. Refinement statistics of both structures are summarized in Table II.

Secondary structures of both PCPs were inspected by the program PROCHECK. Interatomic contacts with a donor-

TABLE I. **Data collection statistics of the wild-type and Cys-free mutant PCPs.** Values in parentheses are for the highest resolution shell.

	*Pf*PCP	*Pf*C142/188S
Detector	Raxis II C	DIP2030
Generator	Rigaku RU-200	Rigaku RU-200
Collimator (mm)	0.3	0.3
Wavelength (Å)	1.5418	1.5418
Monochromator	Graphite	Double-millor
Conditions	40 kV, 100 mA	40 kV, 100 mA
Temperature (°C)	20	20
Distance (mm)	100	200
Step of rotation (deg)	1.5	1.5
Observed reflections	169,460 (10,354)	118,965 (6,425)
Independent reflections	43,412 (4,137)	33,343 (3,349)
Resolution (Å)	200–2.2 (2.3–2.2)	200–2.5 (2.61–2.5)
I/σ (I)	5.8 (2.5)	5.0 (2.8)
Averaged redundancy	3.9 (2.5)	3.6 (1.9)
Completeness (%)	91.5 (69.9)	89.9 (72.0)
R_{merge}	10.1 (31.6)	13.0 (21.1)
Space group	$P2_1$	$P2_1$
Cell parameters		
a (Å)	57.9	49.0
b (Å)	105.0	105.8
c (Å)	78.5	105.8
β (°)	90.7	96.2

TABLE II. **Refinement statistics of the wild-type and Cys-free mutant PCPs.**

	*Pf*PCP	*Pf*C142/188S
Resolution (Å)	10–2.2	10–2.7
Reflections used	40,718	25,840
No. of protein residues	832	832
No. of water molecules	168	124
R factor (%)	19.5	21.0
R_{free} (%)	23.2	24.3
Rmsd from ideality		
Bond length (Å)	0.017	0.025
Bond angles (°)	3.09	3.68
Ramachandran plot statistics		
Residues in most favored region (%)	90.6	89.7
Residues in additionally allowed region (%)	9.2	10.3
Residues in generously allowed region (%)	0.1	0.0
Residues in disallowed region (%)	0.0	0.0
Average B factor		
Main chain (Å²)	37.9	24.5
Side chain (Å²)	44.3	29.5

to-acceptor distance of less than 3.2 Å were assigned as hydrogen bonds. Superposition of the two molecules and estimation of rms deviations between them were performed by the program Biocon.

RESULTS

Quality of the Model—The refinement of *Pf*PCP was converged to an R factor of 19.5% and an R_{free} of 23.2% for reflections in the resolution range 10–2.2 Å. The Cys-free mutant (*Pf*C142/188S) was refined to an R factor of 21.0% and an R_{free} of 24.3% for reflections from 10 to 2.7 Å. Both current models include all 832 residues, 208 residues in each of four subunits, and 168 water molecules for *Pf*PCP and 124 water molecules for *Pf*C142/188S. The refined structure model of *Pf*PCP converged well with rms deviations from the ideal bond length and the angles of 0.017 Å and 3.09°, respectively. 90.6% of the non-glycine residues were in the most favorable region of the Ramachandran plot, 9.2% in the additionally allowed region, and no residues in the disallowed region. Pro159 in each subunit was in a *cis* conformation. The rms deviations from the ideal bond length and the angles for *Pf*C142/188S were 0.025 Å and 3.68°, respectively. 89.7% of the non-glycine residues were in the most favorable region of the Ramachandran plot, 10.3% in the additionally allowed region, and no residues in the disallowed region. The final coordinates have been deposited in the Protein Data Bank (accession No. 1IOF for *Pf*PCP and No. 1IOI for *Pf*C142/188S).

Monomer Structure—The structure of the *Pf*PCP monomer is depicted by a ribbon drawing in Fig. 1a. Monomeric structures of *Ba*PCP and *Tl*PCP superposed on that of *Pf*PCP by the program O (*39*) were drawn by stereoscopic Cα traces using TURBO-FRODO (*34*). The *Pf*PCP monomer folded into a single α/β globular domain. The central β-sheet comprised four-stranded parallel β sheets (β3, β1, β4, and β9), two short two-stranded anti-parallel β sheets (one with β2 and β3, and the other with β5 and β9) and a short parallel β-sheet (β5 and β8). The central β-sheet was sandwiched within five α-helices; two helices (α2 and α4) on one side and three helices (α1, α6, and α3) on the other side. Polypeptide segments from Arg80 to Ser113 and from Tyr169 to Cys188 protruded from the core α/β domain, which are termed the L-shaped protrusion and C-terminal protrusion, respectively, in this paper. The C-terminal protrusion included a 2.5 turn α-helix of α5 and an extended strand. The L-shaped protrusion consisted of a short two-strand anti-parallel β-sheet (β6 and β7) at the horizontal line of L and a distorted anti-parallel β-sheet at the vertical line which was assigned to a loop by the program PROCHECK. Both the C-terminal and the L-shaped protrusions have higher temperature factors than the core domain.

Tetramer Structure—*Pf*PCP exhibits a tetrameric structure similar to that of *Tl*PCP and *Ba*PCP. Individual subunits of *Pf*PCP, termed A, B, C, and D, superpose well on the other subunits related by 222 symmetries within rms displacements less than 0.023 Å for all the main-chain atoms. Three twofold axes were designated the P-, Q-, and R-axes as shown in Fig. 2a. The P-axis relates A to C and D to B, the Q-axis, A to D and C to B, and the R-axis, A to B and C to D. Each subunit of *Pf*PCP is in contact with two

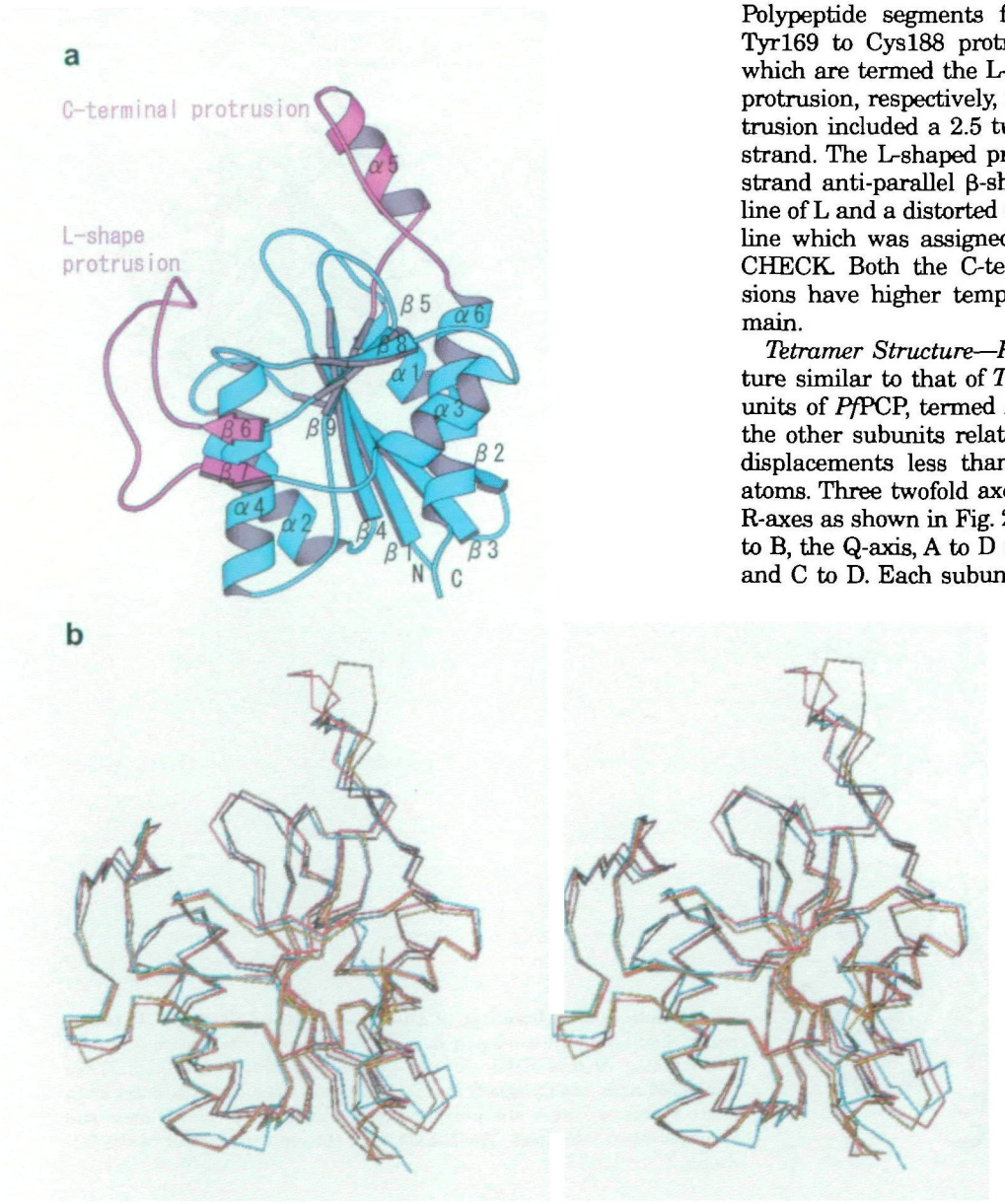

Fig. 1. **(a) A ribbon diagram of the *Pf*PCP monomer with secondary structure elements.** This figure was produced with the program MOLSCRIPT (*38*). **(b) The stereo Cα trace of the *Pf*PCP monomer (red) with the Cα trace of the *Tl*PCP (yellow) and *Ba*PCP (blue) monomers.** This figure was produced with the program TURBO-FRODO (*34*).

other subunits at two different interfaces. One interface, through which the P-axis runs, was designated the P-interface, and the other, around the Q-axis, the Q-interface. The intersubunit contacts in the P-interface are mostly hydrophobic interactions, while those at the Q-interface include ion bonds and hydrophobic interactions.

The hydrophobic contacts between two C-terminal protrusions related by the P-axis are the main intersubunit interactions in the P-interface. Each C-terminal protrusion has an additional intersubunit interaction with a C-terminal end of α3, a loop between an α3 and a β8, a strand of β8, a loop between β4 and β5, and an N-terminal end of α6. Hydrophobic interactions appeared prominent, and no ion bond was detected at the P-axis interface.

The L-shaped protrusion is responsible for intermolecular interactions at the Q-interface. This protrusion interacts with an other L-shaped protrusions, the N-terminal end of α2, the N-terminal end of α3, the C-terminal end of β5, the

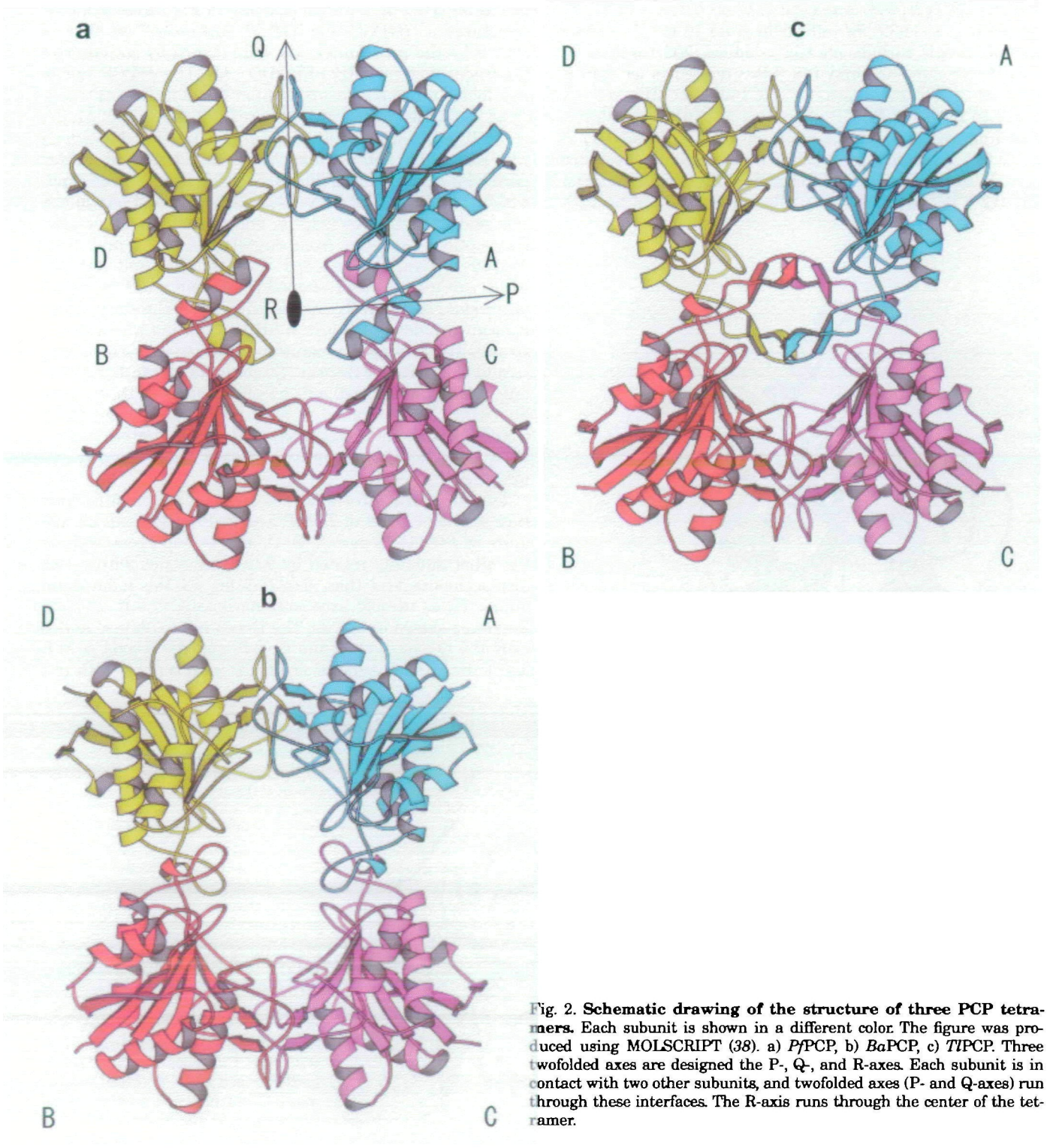

Fig. 2. **Schematic drawing of the structure of three PCP tetramers.** Each subunit is shown in a different color. The figure was produced using MOLSCRIPT (*38*). a) *Pf*PCP, b) *Ba*PCP, c) *Tt*PCP. Three twofolded axes are designed the P-, Q-, and R-axes. Each subunit is in contact with two other subunits, and twofolded axes (P- and Q-axes) run through these interfaces. The R-axis runs through the center of the tetramer.

loop between β5 and β6, the C-terminal end of β8, the loop between β8 and α4, and the N-terminal end of α4. Ten ion bonds were detected at this interface. They were Asp87–Arg80, Asp100–Lys118, Glu99–Lys118, Asp100–Arg80, Asp100–Lys118, and their twofold symmetry-related pairs. In addition to these charged amino acids, Ile81, Val83, Ala85, Thr109, Ala110, Tyr111, Phe112, Ser136, and Leu139 were included in the hydrophobic interactions around the Q-axis.

In *Tf*PCP, Cys190 locates close to the end of the C-terminal protrusion, that is, at the beginning of the C-terminal helix (α6) in each monomer, forms a disulfide bond (A–C and B–D) (*26*). Although *Pf*PCP has Cys188 located at the equivalent position, the existence of an inter-subunit disulfide bond was not observed. The distance of Cys188 Sγ between A and C was 3.77 Å.

*Active Site—Pf*PCP has two cysteine residues, Cys142 and Cys188, one of which (Cys142) is completely conserved in all known PCP sequences. This conserved residue plays a key role in PCP activity. In *Pf*PCP, a nucleophilic Cys142 is located in the beginning of α4 near the central sheet (β5 and β9). A schematic drawing of the *Pf*PCP active site is

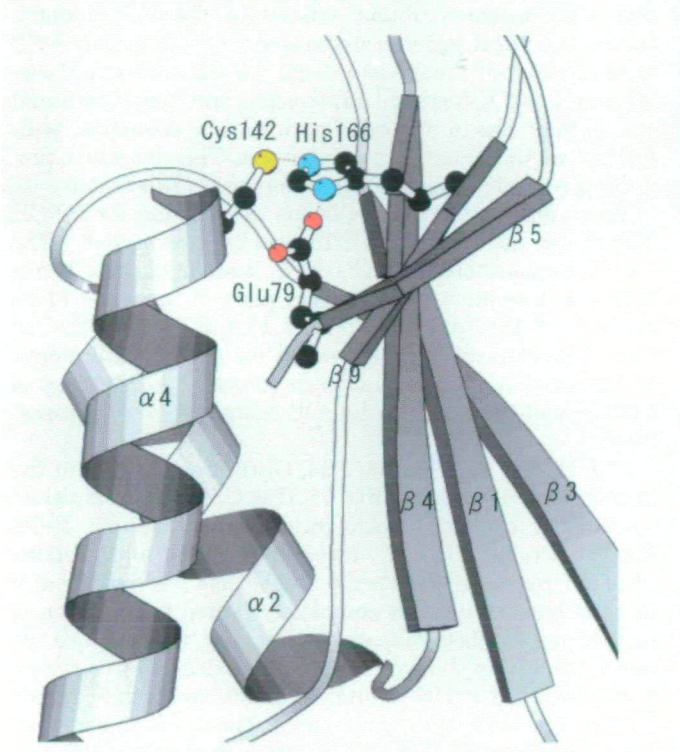

Fig. 3. **Schematic drawing of the *Pf*PCP active site triad Cys142, His166, Glu79.** Cys142 Sγ–His166 Nε1 and His166 Nδ–Cys142 Sγ form hydrogen bonds with distances of 3.49 and 2.72 Å, respectively. The figure was produced using MOLSCRIPT (*38*).

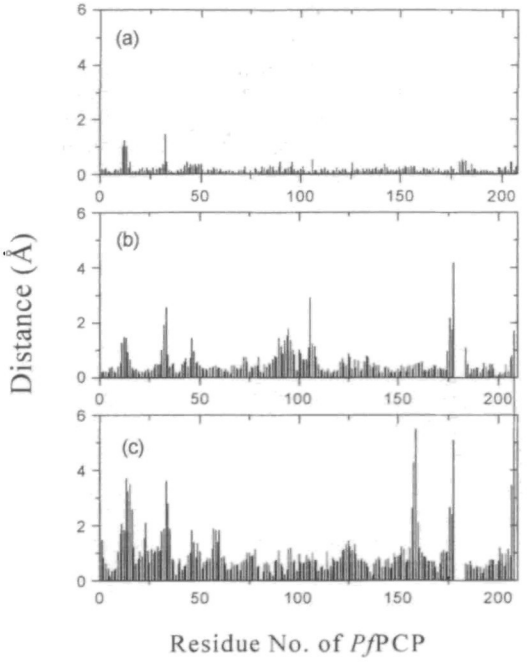

Fig. 4. **Rms deviations of Cα atoms between *Pf*PCP and *Pf*C142/188S (a), between *Pf*PCP and *Tf*PCP (b), and between *Pf*PCP and *Ba*PCP (c) after a least fit of the corresponding Cα atoms.** In the case of (a), all residues (208) were used. In (b) and (c), the residues corresponding to *Pf*PCP (1 to 177 and 184 to 208) were used.

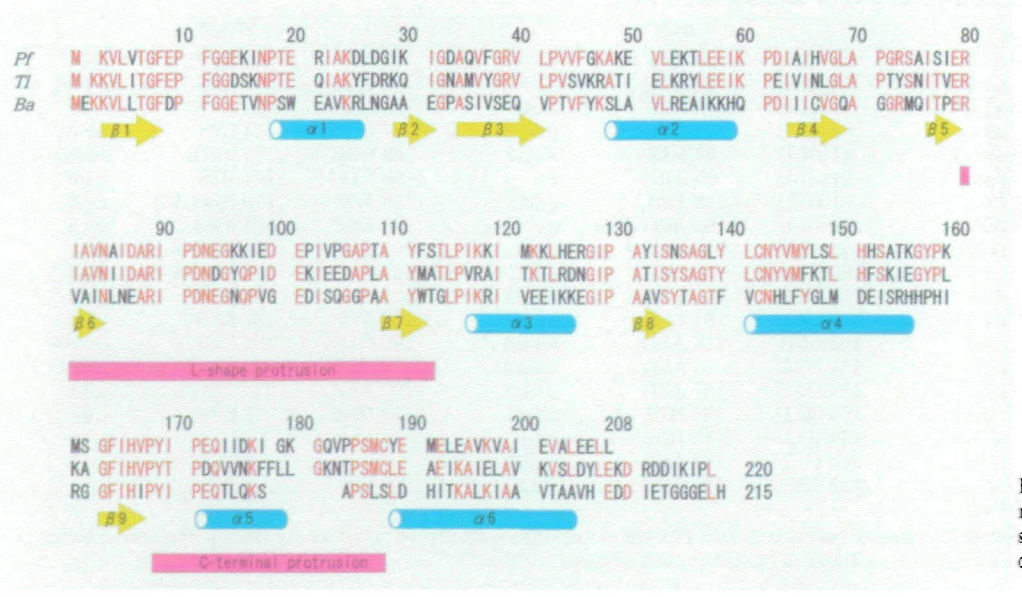

Fig. 5. **The sequence alignments of three PCPs and a schematic drawing of the secondary structure of *Pf*PCP.**

shown in Fig. 3.

His166 located in β9 has also been suggested to be a second component of the Cys-His catalytic dyad. Cys142 Sγ forms a hydrogen bond with His166 Nε1 with a distance of 3.49 Å. Glu79, the third component of a catalytic triad, is located in the loop between β5 and β6. The Glu79 Oε forms a hydrogen bond with His166 Nδ with a distance of 2.72 Å. The sequence of this catalytic triad, Cys-His-Glu, is highly conserved in all known PCP sequences, and its three-dimensional arrangement in *Pf*PCP is consistent with those of other PCP structures.

Structure of PfC142/188S—The overall X-ray structure of the Cys-free mutant PCP is essentially identical to that of the wild-type PCP. The rms deviations for the main chain atoms between *Pf*PCP and *Pf*C142/188S are 0.266 Å. Slight deviations were found in the flexible loops (β1–α1, β2–β3, and α5–α6) as shown in Fig. 4a. The distance (4.74 Å) of Ser188 Oγ between A and C in *Pf*C142/188S was also close to that (3.77 Å) of Cys188 Sγ between A and C in *Pf*PCP. These results indicate that the Cys mutation hardly perturbs the conformation of the wild type PCP, so that *Pf*C142/188S is a very suitable protein for studying the mechanism of the extremely high stability of *Pf*PCP using DSC, because no complexities are introduced into the heat capacity curve in DSC by the Cys residues.

Structural Comparison of Three PCPs—As shown in Fig. 2, large structural variations were detected in the C-terminal protrusion among three PCPs, in which 5 residues were inserted into *Pf*PCP and 6 residues into *Tt*PCP (Fig. 5). Excluding the amino acid residues without equivalent residues among the three PCPs, the rms deviations of the Cα atoms were evaluated. The deviations of *Pf*PCP to *Tt*PCP and *Ba*PCP were 0.726 and 1.399 Å, respectively (Fig. 4). This suggests that *Pf*PCP is closer to *Tt*PCP than to *Ba*PCP in terms of its main-chain folding, corresponding to the sequence homology. Sequence alignments of the three PCPs and a schematic drawing of the secondary structure of *Pf*PCP are shown in Fig. 5. The amino acid sequence of *Pf*PCP shows 39.4% (82/208) homology with that of *Ba*PCP and 56.3% (117/208) homology with the *Tt*PCP sequence.

On the other hand, remarkable differences in the structures between *Pf*PCP and *Tt*PCP were detected in six regions along the sequence, the β1–α1, β2–β3, and β3–α2 turns, the L-shaped protrusion, the C-terminal protrusion, and the C-terminal coil. The largest structural change between *Pf*PCP and *Tt*PCP was detected in the C-terminal protrusion as shown in Fig. 2. This region of *Pf*PCP contacts another subunit at the P-interface, while that of *Tt*PCP interacts with two different subunits at the P- and R-interfaces. The structural difference in the L-shape protrusion between *Pf*PCP and *Tt*PCP is larger than that between *Pf*PCP and *Ba*PCP. This region in all PCPs interacts with another subunit related by Q-axis symmetry. Large structural differences between *Pf*PCP and *Ba*PCP were detected in the β1–α1, β2–β3, β3–α2, α2–β4, and α4–β9 turns, the C-terminal protrusion, and the C-terminal coil. *Pf*PCP has a five-residue insertion compared with *Ba*PCP in the C-terminal protrusion. This insertion produces a remarkable structural difference in this region.

The number of hydrogen bonds per residue for *Pf*PCP, *Tt*PCP, and *Ba*PCP is 2.13, 2.16, and 2.00, respectively. The two hyperthermophile PCPs have more hydrogen bonds than the mesophile PCP. The ion pairs of the three PCPs within 4 Å are listed in Table III. Figure 6 shows the ion pairs between subunits A and D for the three proteins. There are ten ion pairs at each interface in the case of *Pf*PCP, while *Tt*PCP and *Ba*PCP contain 6 and 4, respectively.

In *Pf*PCP, a polar amino acid, Glu192, was found in the interior of the molecule (Fig. 7). This Glu192 is completely surrounded by hydrophobic residues, Pro18, Ile22, Ile76, Val167, Pro168, Ile170, Met187, Ala195, and Val196. Charged residues are usually located on the surface of a protein, but Glu192 was completely buried in the interior, suggesting the destabilization effect. But the distance between the carboxyl oxygen atom of Glu192 and the oxygen atom of Pro168 is 2.95 Å, and the atoms can form hydrogen bonds if the carboxyl is protonated. This buried polar residue is conserved in *Tt*PCP (Glu194) in the hydrophobic surrounding, and its three-dimensional arrangement is also

TABLE III. **Ion pairs in three PCPs from different sources within 4 Å.**

*Pf*PCP				*Ba*PCP				*Tt*PCP		
14 GLU	177 LYS		c-α5	23 GLU	26 LYS		α1-α1	15 ASP	178 LYS		c-c
20 GLU	24 LYS		α1-α1	23 GLU	27 ARG		α1-α1	21 GLU	25 LYS		α1-α1
27 ASP	39 ARG		α1-β3	33 GLU	194 LYS		c-α6	28 ASP	40 ARG		c-β3
53 GLU	152 HIS		α2-α4	41 GLU	60 LYS		β2-α2	58 GLU	54 LYS		α2-α2
57 GLU	156 LYS		α2-α4	41 GLU	61 HIS		β2-α2	59 GLU	55 ARG		α2-α2
62 ASP	2 LYS		β4-c	81 GLU	75 ARG		c-c	80 GLU	167 HIS		c-β9
62 ASP	160 LYS		β4-c	81 GLU	168 HIS		c-β6	88 ASP	119 ARG	A–D	c-α3
79 GLU	73 ARG		β5-c	89 GLU	82 ARG	A–D	c-c	95 ASP	48 ARG		c-α2
79 GLU	166 HIS		β5-β9	89 GLU	120 LYS	A–D	c-α3	101 ASP	81 ARG	A–D	c-c
87 ASP	80 ARG	A–D	c-c	96 GLU	49 LYS		c-α2	101 ASP	119 ARG	A–D	c-α3
87 ASP	118 LYS	A–D	c-α3	124 GLU	127 LYS		α3-α3	105 GLU	152 HIS		c-α4
99 GLU	97 LYS		c-c	129 GLU	191 LYS		c-α6	127 ASP	123 LYS		α3-α3
99 GLU	118 LYS	A–D	c-α3	153 ASP	157 ARG		α4-α4	199 GLU	196 LYS		α6-α6
100 ASP	80 ARG	A–D	c-c	154 GLU	55 ARG		α4-α2	199 GLU	203 LYS		α6-α6
100 ASP	118 LYS	A–D	c-α3	154 GLU	157 ARG		α4-α4	207 ASP	213 ARG		α6-c
172 GLU	21 ARG		α5-α1	154 GLU	158 HIS		α4-c	210 GLU	2 LYS		α6-c
176 ASP	177 LYS		α5-α5	154 GLU	159 HIS		α4-c				
194 GLU	127 ARG		α6-c	204 GLU	163 ARG		c-β6				
201 GLU	127 ARG		α6-c	205 ASP	121 ARG		c-α3				
206 GLU	119 LYS		c-α3								

A–D represents an inter-subunit ion pair between subunits A and D. Others are intra-subunit ion pairs in subunit A. The last column in each PCP shows the location of the ion pairs (α, α-helix; β, β-sheet; c, coil or turn).

Fig. 6. **Comparison of ion pairs between subunits A and D for the three proteins, *Pf*PCP (a), *Ba*PCP (b), *Tl*PCP (c).** There are ten salt bridges at each interface in *Pf*PCP, Asp80–Arg87, Asp87–Lys118, Glu99–Lys118, Asp100–Arg80, and Asp100–Lys118, and its noncrystallographic symmetry-related pairs form salt bridge interactions. The figure was produced using MOLSCRIPT (*38*).

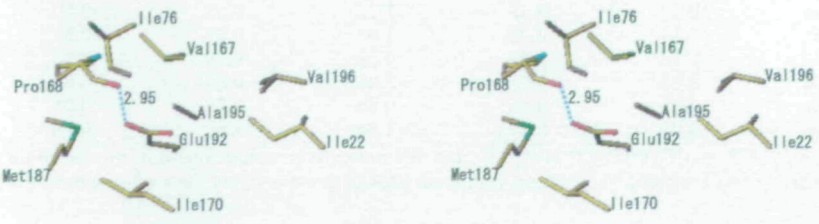

Fig. 7. **The structure surrounding glutamic acid 192 of *Pf*PCP in the hydrophobic interior of a molecule.** The distance between the carboxyl oxygen atom of Glu192 and the oxygen atom of Pro168 is 2.62 Å.

similar to that in *Pf*PCP. On the other hand, the corresponding residue in *Ba*PCP is Ile189, and it is also in the hydrophobic interior.

DISCUSSION

The thermal stability of *Pf*PCP is very high compared with that of *Ba*PCP: the peak temperatures of the DSC curves at pH 9.5 are 104.5°C for *Pf*PCP and 62.9°C for *Ba*PCP (*23*). If Cys188 in *Pf*PCP forms a disulfide bond between subunits, the stability further increases: the peak temperature of the DSC curve is 116.5°C at pH 9.5. On the other hand, *Tl*PCP seems to be less stable than *Pf*PCP (a half-life of 2 h at 75°C (*26*), although it comes from a hyperthermophile archaeon. The stabilization mechanism of *Pf*PCP was investigated on the basis of structural differences among the three proteins, *Pf*PCP, *Tl*PCP, and *Ba*PCP.

Contribution of the Hydrophobic Interaction—Hydrophobic interactions in the interior of a protein are among the important stabilizing forces (*40*). In experiments using a series of hydrophobic mutants of human lysozyme, Takano *et al.* (*41*) have found a general rule for the relationship between a hydrophobic effect and the conformational stability of a protein. The change in the unfolding Gibbs energy (ΔG) due to a hydrophobic effect between wild-type and mutant proteins ($\Delta\Delta G_{HP}$) can be expressed using changes in the accessible surface area (ASA) of non-polar and polar atoms due to denaturation as follows (*42*):

$$\Delta\Delta G_{HP} = \alpha\Delta\Delta ASA_{non\text{-}polar} + \beta\Delta\Delta ASA_{polar} \quad (1)$$

where $\Delta\Delta ASA_{non\text{-}polar}$ and $\Delta\Delta ASA_{polar}$ represent the differences between wild-type and mutant proteins in ΔASA of the non-polar and polar atoms, respectively, of all residues upon denaturation. Using the stability/structure database for a series of mutant human lysozymes, the parameters α and β have been determined to be 0.178 and –0.013 kJ mol^{-1} Å^{-2}, respectively (*42*). ASA values of proteins in the native state can be calculated using X-ray crystal structures, and those in the denatured state using their extended structures. For the calculation of ASA, C/S atoms in residues were assigned to $ASA_{non\text{-}polar}$ and N/O to ASA_{polar}.

We tried to estimate the contribution of hydrophobic interactions in *Pf*PCP, *Tl*PCP, and *Ba*PCP to the stabilization ($\Delta\Delta G_{HP}$). From the X-ray crystal structures of the three proteins in the native state, *ASA* values were calculated by the procedure of Connolly (*43*). The *ASA* values in the

TABLE IV. **The contribution of hydrophobic interactions to the conformational stability of three PCPs.**

Protein	ΔASA(C/S)	ΔASA(N/O)	ΔG_{HP}	$\Delta\Delta G_{HP}$
*Ba*PCP	13,530	5,997	2,330	
4*Ba*PCP*	58,545	25,838	2,521	
*Tl*PCP	14,874	5,950	2,570	240
4*Tl*PCP*	65,800	26,794	2,841	320
*Pf*PCP	13,860	5,672	2,393	63
4*Pf*PCP*	59,430	24,728	2,564	43

ΔASA values are Å^2; ΔG is in kJ/mol of monomer. $\Delta\Delta G_{HP}$ represents the difference in ΔG_{HP} between mesophile and hyperthermophile proteins. *Tetramer PCP.

TABLE V. **SPMP stability scores of each PCP structure.**

a) Monomer

Structure	Total	SP	Hyd	LC	BR
*Ba*PCP	400.8	302.0	50.6	106.6	−58.1
*Tl*PCP	419.2	314.2	46.8	122.5	−64.4
*Pf*PCP	455.2	306.6	70.2	136.3	−58.1
Tl–Ba	18.4	12.1	−3.7	15.4	−6.2
Pf–Ba	54.3	5.0	19.6	29.2	0

b) Tetramer

Structure	Total	SP	Hyd	LC	BR
4 *Ba*PCP	423.4	320.0	58.1	106.6	−61.9
4 *Tl*PCP	468.1	353.5	60.6	122.5	−68.6
4*Pf*PCP	490.3	321.3	93.3	136.3	−61.0
4*Tl–4Ba*	44.7	33.4	2.5	15.8	−6.6
4*Pf–4Ba*	66.9	1.2	35.1	29.7	0.8

Units are kJ/mol. Positive values show stabilization. *Pf–Ba* and *Tl–Ba* represent the difference in total scores between *Pf*PCP and *Ba*PCP, and between *Tl*PCP and *Ba*PCP, respectively. SP, Hyd, LC, and BR are contributions due to side-chain packing ($\Delta\Delta G_{SP}$), hydration ($\Delta\Delta G_{Hyd}$), local structure ($\Delta\Delta G_{LC}$) and back-bone-side-chain repulsion ($\Delta\Delta G_{BR}$), respectively, for each residue (Eq. 2).

TABLE VI. **The top ten residues in terms of difference in SPMP scores between *Pf*PCP and *Ba*PCP.**

No.	*Pf–Ba*	Protein	Site	Total	SP	Hyd	LC	BR
1	9.83	*Pf*PCP	31Ile	5.36	2.89	0.96	1.63	−0.13
		*Ba*PCP	33Glu	−4.48	−1.76	−1.21	−1.38	−0.13
2	7.45	*Pf*PCP	169Tyr	2.47	5.48	0.59	−0.63	−3.01
		*Ba*PCP	171Tyr	−4.98	−1.84	−0.13	−0.79	−2.18
3	6.40	*Pf*PCP	105Pro	6.23	0.46	1.42	4.39	0
		*Ba*PCP	107Gln	−0.17	0.17	0.54	−0.88	−0.04
4	6.07	*Pf*PCP	132Tyr	5.10	2.43	1.05	1.80	−0.21
		*Ba*PCP	134Ala	−0.96	−0.29	−0.25	−0.46	0
5	5.94	*Pf*PCP	78Ile	7.03	4.27	1.51	1.63	−0.42
		*Ba*PCP	80Pro	1.09	2.72	−0.96	−0.63	−0.08
6	5.56	*Pf*PCP	205Glu	2.05	−0.18	1.21	1.09	−0.08
		*Ba*PCP	202Val	−3.51	0.08	−1.21	−2.13	−0.25
7	5.48	*Pf*PCP	193Leu	2.22	2.93	−1.55	1.09	−0.25
		*Ba*PCP	190Thr	−3.26	−0.75	0.29	−2.64	−0.17
8	5.31	*Pf*PCP	124Leu	10.42	8.58	1.72	0.63	−0.50
		*Ba*PCP	126Ile	5.10	3.26	1.88	0.67	−0.67
9	5.02	*Pf*PCP	152His	2.18	2.05	−0.54	0.79	−0.13
		*Ba*PCP	154Glu	−2.85	−0.75	−2.05	0.84	−0.84
10	4.77	*Pf*PCP	151His	4.43	3.43	0.29	0.79	−0.08
		*Ba*PCP	153Asp	−0.33	3.47	−1.84	−1.80	−0.13

Pf–Ba represents the difference in total scores between *Pf*PCP and *Ba*PCP. SP, Hyd, LC, and BR indicate contributions due to side-chain packing ($\Delta\Delta G_{SP}$), hydration ($\Delta\Delta G_{Hyd}$), local structure ($\Delta\Delta G_{LC}$) and back-bone-side-chain repulsion ($\Delta\Delta G_{BR}$), respectively, for each residue (Eq. 2). The units of score are kJ/mol.

denatured states were calculated from the extended structures of each protein, which were generated from the native structures using Insight II. As shown in Table IV, the ΔG values due to hydrophobic interactions (ΔG_{HP}) of *Pf*PCP were greater than those of *Ba*PCP: the $\Delta\Delta G_{HP}$ values between *Pf*PCP and *Ba*PCP were 63 and 43 kJ/mol per monomer, assuming a monomer in the native state and a tetramer in the native state, respectively. However, the $\Delta\Delta G_{HP}$ values for *Pf*PCP were smaller than those of *Tl*PCP. These results indicate that the higher stabilities of *Pf*PCP and *Tl*PCP are caused by hydrophobic interactions. The contents of hydrophobic residues (total of Ile, Val, Leu, Phe, Cys, Met, and Ala) are 41.9, 40.0, 37.7% for *Pf*PCP, *Tl*PCP, and *Ba*PCP, respectively. Although the content in *Tl*PCP is not the highest, the higher hydrophobic effect of *Tl*PCP might come from buried hydrophobic ethylene groups on Lys and Arg, which contribute to the hydrophobic interactions.

Stability Analysis of the PCP Structures by Knowledge-Based Potential—Ota *et al.* (*44*) have proposed that the changes in conformational stability due to a single amino acid substitution can be calculated by SPMP (stability profiles of mutant proteins) using the X-ray structures. In SPMP, the pseudo-energy potential ($\Delta\Delta G_{SPMP}$) developed for evaluating structure-sequence compatibility in the structure prediction method is employed, consisting of four elements: side-chain packing ($\Delta\Delta G_{SP}$), hydration ($\Delta\Delta G_{Hyd}$), local structure ($\Delta\Delta G_{LC}$), and back-bone-side-chain repulsion ($\Delta\Delta G_{BR}$) (*44*, *45*).

$$\Delta\Delta G_{SPMP} = \Delta\Delta G_{SP} + \Delta\Delta G_{Hyd} + \Delta\Delta G_{LC} + \Delta\Delta G_{BR} \quad (2)$$

The pseudo-energy potential provides a fitness score for each residue type at a site in a native structure. The estimation of $\Delta\Delta G$ for a replacement of residue X by residue Y is as follows.

$$\begin{aligned}\Delta G(X) &= \langle G(X)\rangle - G(X) \\ &= G^D(X) - G^N(X) \quad (3)\\ \Delta\Delta G(X\rightarrow Y) &= \Delta G(Y) - \Delta G(X) \\ &= [G^D(Y) - G^N(Y)] - [G^D(X) - G^N(X)] \\ &= [G^D(Y) - G^D(X)] - [G^N(Y) - G^N(X)] \quad (4)\end{aligned}$$

where $G(X)$ and $\langle G(X)\rangle$ represent the fitness scores for residue X at a site in the native structure calculated by the potential and the reference score, respectively, corresponding to the Gibbs energy in the native and denatured states for residues X, $G^N(X)$, and $G^D(X)$, respectively.

The conformational stabilities of the three PCP structures were analyzed by SPMP. The individual stability score of four terms are summarized in Table V. The difference in the total score of the PCPs from hyperthermophiles and the mesophile, *e.g.*, *Tl–Ba* and *Pf–Ba*, explains the significant stability of both hyperthermophile PCPs very well; however, the contributions of each score term differ slightly. *Tl*PCP appears to be stabilized mainly by the side-chain packing term, while the hydration and local structural terms are the contributors to *Pf*PCP stabilization. Although it is not easy to interpret the side-chain packing and hydration terms individually because both originate from hydrophobic interactions, it seems that the packing pattern of *Pf*PCP is simpler than that of *Tl*PCP: hydrophobic and hydrophilic residues are located on the interior or exterior of the protein structure, respectively, and *Tl*PCP has a more preferable side-chain arrangement than *Pf*PCP. On the basis of a tetramer conformation, the stability score of *Pf*PCP was also the highest, as shown in Table Vb.

The fitness of the PCP sequence at each position was estimated by the knowledge-based function (SPMP). Comparing the stability score of each residue of *Pf*PCP with that of the corresponding residue in *Ba*PCP, the residues important for the conformational stability of *Pf*PCP can be determined. The top 10 differences are listed in Table VI, suggesting which residues of *Pf*PCP contribute to the stability as compared with *Ba*PCP.

The largest difference in the stability scores is between Ile31 of *Pf*PCP and Glu33 of *Ba*PCP. Ile31 is involved in a β strand and Ile exhibits strong β intensity. Also, Ile 31 interacts with Ile29, Val36, Ile200, and Ile204, and they constitute a small hydrophobic cluster near the protein surface. On the other hand, Glu33 of *Ba*PCP interacts only with Lys194 and they form a salt-bridge. Tyr169 of *Pf*PCP (Tyr171 of *Ba*PCP) increases the score by interactions with Gln14, Pro71, and Lys177. On the other hand, Tyr171 and Gly73 appear too close in the *Ba*PCP structure. Pro105 of *Pf*PCP (Gln107 of *Ba*PCP) is very suitable for the local structure around this site: extended coil (position 104)–extended coil (position 105)–left-handed helix (position 106). Tyr132 of *Pf*PCP (Ala134 of *Ba*PCP) in the A chain interacts with Ala75 and Ser77 in the same chain and Val183 in the C chain. Moreover, the β propensity of Tyr is preferable to that of Ala. Ile78 of *Pf*PCP (Pro80 of *Ba*PCP) is in a hydrophobic environment: Ile171, Ile120, Met121, Leu124, Ile113, and Ile165. Around Pro80 in *Ba*PCP, there are also Ile119, Ile122, and Ile167, yet the interactions are less than in the former case. Glu205 of *Pf*PCP (Val202 of *Ba*PCP), on the helix C-terminal and partially buried, is more suitable than Val. Leu124 of *Pf*PCP (I126 in *Ba*PCP) interacts with more hydrophobic residues (Ile76, Ile78, Ile120, Ile129, Ala131, Ala195, and Val198) than Ile126 in *Ba*PCP (Ile78, Ile131, Ala133, and Ile195).

SPMP provides stability scores for each residue at every site. In the case of *Pf*PCP (208 amino acid residues), the stability changes upon mutation. $\Delta\Delta G$ values for 208 × 19 mutants were predicted by SPMP (*44*) using the crystal structure of *Pf*PCP. 30.3% of the native residues of *Pf*PCP rank at the top of 20 kinds of residues, while the percentage in *Ba*PCP is 27.9%. The average ranking of all native residues among 20 amino acids for *Pf*PCP and *Ba*PCP is 4.95 and 5.74, respectively. These results indicate that the sequence of the hyperthermophile protein (*Pf*PCP) is more fitted to an ideal structure than that of the mesophile protein (*Ba*PCP).

Contribution of Ion Pairs (Salt Bridges)—In hyperthermophile proteins, ion pair networks on the protein surface are usually assumed to be stabilizing (*4*, *9*, *46*). Table III lists the ion pairs formed within 4 Å in the three PCPs. The number (0.10) of ion pairs per residue for *Pf*PCP is similar to that (0.09) for *Ba*PCP but greater than that (0.07) for *Tl*PCP. All values are greater than the average number (0.04) in mesophile proteins (*47*). In *Pf*PCP, 31 residues are involved in the formation of 20 ion pairs: 6 ion pairs with 6 residues form an ion pair network between subunits (A and D, or B and C) (Fig. 6a). In *Ba*PCP, 5 ion pairs involving 6 residues form an intramoleculer ion network. *Tl*PCP has only a small ion network between subunits (4 ion pairs involving 5 residues). An intramoleculer ion-network in a mesophilic protein (*Ba*PCP), which is almost buried in the

interior of the molecule, disappears in hyperthermophile proteins (*Pf*PCP and *Tl*PCP). Ion pairs between subunits A and D are partly conserved in the three proteins, but those in *Pf*PCP form an intersubunit network and seem to contribute to the higher stability of the tetramer (Fig. 6).

Contribution of Hydrogen Bonds—Hydrogen bonds are ubiquitous in proteins, and their contribution to conformational stability is of fundamental importance, as are hydrophobic interactions. Recently, the net contribution of an intramolecular hydrogen bond has been estimated to be 8.5 kJ/mol for a 3 Å–long hydrogen bond as determined using a series of hydrogen bond mutants of human lysozyme (*48*). The average number of hydrogen bonds per residue in *Pf*PCP, *Tl*PCP, and *Ba*PCP is 2.086, 2.064, and 1.986, respectively. The total number of hydrogen bonds in *Pf*PCP (434/208 residues) is greater than in *Ba*PCP (417/210 residues) but comparable to that in *Tl*PCP (454/220 residues). The increase in 17 hydrogen bonds corresponds to a stabilization of 144 kJ/mol. These results suggest that the hydrogen bonds of both hyperthermophile proteins contribute considerably to their higher thermostabilities compared with the mesophile protein. In addition to intrasubunit hydrogen bonds, there are 10, 14, and 2 intersubunit hydrogen bonds in *Pf*PCP, *Tl*PCP, and *Ba*PCP, respectively. This indicates that both hyperthermophile proteins are also more stabilized by subunit interactions through hydrogen bonding than the mesophile protein.

Other Contributions to Stability—Important stabilizing factors include entropic effects when the conformational entropy of a protein is decreased in the denatured state due to substitutions or deletion. Entropic effects correspond to the introduction of disulfide bonds, substitution of other residues with Pro, and the shortening of polypeptides. The X-ray structure of *Pf*PCP indicates that Cys188 in *Pf*PCP does not form a disulfide bond, although the corresponding Cys190 in *Tl*PCP does (*26*). *Pf*PCP is expressed in an *E. coli* strain that clones only the PCP gene from *P. furiosus*. Cys188 is partly oxidized during the purification process, and the resulting oxidized *Pf*PCP shows greater stability than the not-oxidized *Pf*PCP (*23*). The X-ray structure of *Pf*PCP also indicates that Cys188 is capable of forming a disulfide bond between subunits. Therefore, the *Pf*PCP expressed under physiological conditions in *P. furiosus* at around 100°C might form an intersubunit disulfide bond at Cys188 that stabilizes the conformation.

The number of Pro residues is 15 or 16 in the three proteins, suggesting that there is no difference in stability due to Pro content. The number of residues in *Pf*PCP, *Tl*PCP, and *Ba*PCP is 208, 220, and 215, respectively. The entropic effects of denaturation can be calculated from their amino acid compositions using thermodynamic parameters proposed by Oobatake and Ooi (*49*): the denaturation entropy for *Pf*PCP, *Tl*PCP, and *Ba*PCP is 0.67, 0.67, and 0.40, kJ mol^{-1} K^{-1}, respectively. This indicates that neither hyperthermophile protein is stabilized by its entropic effects.

The increase in cavity volume in the interior of a protein decreases the conformational stability. The contribution (ΔG) of the changes in the cavity volume to protein stability has been estimated to be −0.100 and −0.073 kJ mol^{-1} $Å^{-3}$, using mutant T4 lysozymes (*50*) and data for both mutant human and T4 lysozymes (*51*), respectively. For tetramers of the three PCPs, the cavity volume was determined by attempting to insert a probe sphere with a radius of 1.4 Å (assuming a water molecule) (*43*). The total volume of the cavity for *Pf*PCP, *Tl*PCP, and *Ba*PCP is 973, 622, and 1,129 $Å^3$, respectively. This result indicates that *Tl*PCP is stabilized considerably by the decrease in cavity volume, but *Pf*PCP is comparable to *Ba*PCP.

Ionized amino acids in globular proteins are almost exclusively on the outside exposed to the solvent. They are believed to form ion pairs or play essential roles in function (including catalysis and stability) when in the interior of a protein. Glu192 in *Pf*PCP is 100% buried in the hydrophobic core, and the corresponding Glu194 in *Tl*PCP is also completely buried, suggesting that the buried Glu residue is conserved in hyperthermophiles. On the other hand, the corresponding residue in the mesophile protein *Ba*PCP is a hydrophobic residue, Ile195, which might play an important role in hydrophobic interactions. Both Glu residues in the hyperthermophiles, which do not have any ion pairs, seem to contribute to destabilizing the protein. If the Glu residues are replaced by hydrophobic residues, the mutant protein should be stabilized. However, all *Pf*PCPs with hydrophobic mutations at Glu192 are less stable than the wild-type protein (in this case Cys-free *Pf*PCP was used) (in preparation). The OE1 atom of Glu192 in *Pf*PCP is close to the O atom of Pro168 (2.95 Å): the OE2 atom of Glu194 in *Tl*PCP is also close to the O atom of Pro169 (2.62 Å). This suggests that if Glu192 (Glu194) is protonated, the protonated Glu might form a hydrogen bond with the O atom of Pro. However, at present, it is difficult to explain how the conserved buried Glu residues in hyperthermophiles play an important role in stabilization.

Conclusions—The crystal structures of pyrrolidone carboxyl peptidases from *P. furiosus* and its Cys-free mutant were determined at 2.2 and 2.7 Å, respectively. The extremely high stability of the protein could be explained on the basis of its structure and those of two homologous structures from a hyperthermophile and a mesophile. The high stability of *Pf*PCP is due to increases in hydrophobic interactions and hydrogen bonds, the formation of an intersubunit ion pair network, and improvement to an ideal conformation. On the other hand, the stabilization of *Tl*PCP is mainly caused by a remarkable increase in hydrophobic interactions and a decrease in denaturation entropy due to the formation of disulfide bonds. From these results and those previously reported, we can conclude that a hyperthermophile protein does not have special factors responsible for its extremely high stability, and that the conformational structure is superior in the combination of positive and negative factors for stabilization compared to a mesophile protein.

REFERENCES

1. Pace, C.N., Shirley, B.A., McNutt, M., and Gajiwala, K. (1996) Forces contributing to the conformational stability of proteins. *FASEB J.* **10**, 75–83
2. Tanner, J., Hecht, R.M., and Krause, K.L. (1996) Determinants of enzyme thermostability observed in the molecular structure of *Thermus aqaticus* D-glyceraldehyde-3-phosphate dehydrogenase at 2.5 Å resolution. *Biochemistry* **35**, 2597–2609
3. Aguilar, C.F., Sanderson, I., Moracci, M., Ciaramella, M., Nucci, R., Rossi, M., and Pearl, L.H. (1997) Crystal structure of the β-glycosidase from the hyperthermophilic archaeon *Sulfolobus solfataricus*: resilience as a key factor in thermostability. *J. Mol. Biol.* **271**, 789–802

4. Hening, M., Darimont, B., Sterner, R., Kirschner, K., and Jansonius, J.N. (1995) 2.0 Å structure of indole-3-glycerolphosphate synthase from the hyperthermophile *Sulfolobus solfataricus*: possible determinants of protein stability. *Structure* **3**, 1295–1306
5. Hening, M., Sterner, R., Kirschner, K., and Jansonius, J.N. (1997) Crystal structure at 2.0 Å resolution of phosphoribosyl anthranilate isomerase from the hyperthermophile *Thermotoga maritima*: possible determinants of protein stability. *Biochemistry* **36**, 6009–6016
6. Knapp, S., de Vos, W.M., Rice, D., and Ladenstein, R. (1997) Crystal structure of glutamate dehydrogenase from the hyperthermophilic eubacterium *Thermotoga maritima* at 3.0 Å resolution. *J. Mol. Biol.* **267**, 916–932
7. Korndorfer, I., Steipe, B., Huber, R., Tomschy, A., and Jaenicke, R. (1995) The crystal structure of holo-glyceraldehyde-3-phosphate dehydrogenase from the hyperthermophilic bacterium *Thermotoga maritima* at 2.5 Å resolution. *J. Mol. Biol.* **246**, 511–521
8. Russell, R.J.M., Ferguson, J.M.C., Hough, D.W., Danson, M.J., and Taylor, G.L. (1997) The crystal structure of citrate synthase from the hyperthermophilic archaeon *Pyrococcus furiosus* at 1.9 Å resolution. *Biochemistry* **36**, 9983–9994
9. Yip, K.S.P., Stillman, T.J., Britton, K.L., Artymiuk, P.J., Baker, P.J., Sedelnikova, S.E., Engel, P.C., Pasquo, A., Chiaraluce, R., and Consalvi, V. (1995) The structure of *Pyrococcus furiosus* glutamate dehydrogenase reveals a key role for ion-pair networks in maintaining enzyme stability at extreme temperatures. *Structure* **3**, 1147–1158
10. Tahirov, T.H., Oki, H., Tsukihara, T., Ogasahara, K., Yutani, K., Ogata, K., Izu, Y., Tsunasawa, S., and Kato, I. (1998) Crystal structure of methionine aminopeptidase from hyperthermophile, *Pyrococcus furiosus*. *J. Mol. Biol.* **284**, 101–124
11. Yamagata, Y., Ogasahara, K., Hioki, Y., Lee, S.J., Nakagawa, A., Nakamura, H., Ishida, M., Kuramitsu, S., and Yutani, K. (2001) Entropic stabilization of the tryptophan synthase alpha-subunit from a hyperthermophile, *Pyrococcus furiosus*: X-ray analysis and calorimetry. *J. Biol. Chem.* **276**, 11062–11071
12. Spassov, V.Z., Karshikoff, A.D., and Ladenstein, R. (1995) The optimization of protein-solvent interactions: thermostability and the role of hydrophobic and electrostatic interactions. *Protein Sci.* **4**, 1516–1527
13. Schumann, J., Bohm, G., Schumacher, G., Rudolph, R., and Jaenicke, R. (1993) Stabilization of creatinase from *Pseudomonas putida* by random mutagenesis. *Protein Sci.* **12**, 1612–1620
14. Russell, R.J.M., Hough, D.W., Danson, M.J., and Taylor, G.L. (1994) The crystal structure of citrate synthase from the thermophilic archaeon *Thermoplasma acidophlum*. *Structure* **2**, 1157–1167
15. Britton, K.L., Baker, P.J., Borges, K.M., Engel, P.C., Pasquo, A., Rice, D.W., Robb, F.T., Scandurra, R., Stillman, T.J., and Yip, K.S. (1995) Insights into thermal stability from a comparison of the glutamate dehydrogenases from *Pyrococcus furiosus* and *Thermococcus litoralis*. *Eur. J. Biochem.* **229**, 688–695
16. Jaenicke, R., Schurig, H., Beaucamp, N., and Ostendorp, R. (1996) Structure and stability of hyperstable proteins: Glycolytic enzymes from hyperthermophilic bacterium *Thermotoga maritima*. *Adv. Protein Chem.* **48**, 181–269
17. Jaenicke, R. and Bohm, G. (1998) The stability of proteins in ex-treme environments. *Curr. Opin. Struct. Biol.* **8**, 738–748
18. Sterner, R., Kleemann, G.R., Szadkowski, H., Lustig, A., Hennig, M., and Kirschner, K. (1996) Phosphoribosyl anthranilate isomerase from *Thermotoga maritima* is an extremely stable and active homodimer. *Protein Sci.* **5**, 2000–2008
19. Villeret, V., Clantin, B., Tricot, C., Legrain, C., Roovers, M., Stalon, V., Glansdorff, N., and Van Beeumen, J. (1998) The crystal structure of *Pyrococcus furiosus* ornithine carbamoyltransferase reveals a key role for oligomerization in enzyme stability at extremely high temperatures. *Proc. Natl. Acad. Sci. USA* **95**, 2801–2806
20. Hess, D., Kruger, K., Knappik, A., Palm, P., and Hensel, R. (1995) Dimeric 3-phosphoglycerate kinases from hyperthermophilic Archaea. Cloning, sequencing and expression of the 3-phosphoglycerate kinase gene of *Pyrococcus woesei* in *Escherichia coli* and characterization of the protein. Structural and functional comparison with the 3-phosphoglycerate kinase of *Methanothermus fervidus*. *Eur. J. Biochem.* **233**, 227–237
21. Dams, T. and Jaenicke, R. (1999) Stability and folding of dihydrofolate reductase from the hyperthermophilic bacterium *Thermotoga maritima*. *Biochemistry* **38**, 9169–9178
22. Ogasahara, K., Nakamura, M., Nakura, S., Tsunasawa, S., Kato, I., Yoshimoto, T., and Yutani, K. (1998) The unusually slow unfolding rate causes the high stability of pyrrolidone carboxyl peptidase from a hyperthermophile, *Pyrococcus furiosus*: Equilibrium and kinetic studies of guanidine hydrochloride-induced unfolding and refolding. *Biochemistry* **37**, 17537–17544
23. Ogasahara, K., Khechinashvili, N.N., Nakamura, M., Yoshimoto, T., and Yutani, K. (2001) Thermal stability of pyrrolidone carboxyl peptidases from hyperthermophilic archaeon, *Pyrococcus furiosus*. *Eur. J. Biochem.* **268**, 3233–3242
24. Knapp, S., Karshikoff, A., Berndt, K.D., Christova, P., Atansov, B., and Ladenstein, R. (1996) Thermal unfolding of the DNA-binding protein Sso7d from the hyperthermophile *Sulfolobus solfataricus*. *J. Mol. Biol.* **264**, 1132–1144
25. McCrary, B.S., Edomondson, S.P., and Shriver, J.W. (1996) Hyperthermophile protein folding thermodynamics: Differential scanning calorimetry and chemical denaturation of Sac7d. *J. Mol. Biol.* **264**, 784–805
26. Singleton, M.R., Isupov, M.N., and Littlechild, J.A. (1999) X-ray structure of pyrrolidone carboxyl peptidase from the hyperthermophilic archaeon *Thermococcus litoralis*. *Structure* **7**, 237–244
27. Odagaki, Y., Hayashi, A., Okada, K., Hirotsu, K., Kabashima, T., Ito, K., Yoshimoto, T., Tsuru, D., Sato, M., and Clardy, J. (1999) The crystal structure of pyroglutamyl peptidase I from *Bacillus amyloliquefaciens* reveals a new structure for a cysteine protease. *Structure* **7**, 399–411
28. Otwinowski, Z. and Minor, W. (1997) Processing of X-ray diffraction data collected in oscillation mode in *Methods in Enzymology* (Carter Jr., C.W. and Sweet, R.W., eds.) Vol. 276, pp. 307–326, Academic Press, New York
29. Wang, B.C. (1985) Resolution of phase ambiguity in macromolecular crystallography. *Methods Enzymol.* **115**, 90–112
30. Zhang, K.Y.J. and Main, P. (1990) The use of Sayre's equation with solvent flattening and histogram matching for phase extension and refinement of protein structures. *Acta Cryst.* **A46**, 377–381
31. Bricogne, G. (1974) Geometric sources of redundancy in intensity data and their use for phase determination. *Acta Cryst.* **A30**, 395–405
32. Schuller, D. (1996) More versatile non-crystallographic averaging with multiple constraints. *Acta Cryst.* **D52**, 425–434
33. Collaborative Computational Project, Number 4 (1994) The CCP4 suite: programs for protein crystallography. *Acta Cryst.* **D50**, 760–763
34. Jones, T.A. (1985) Diffraction methods for biological macromolecules. Interactive computer graphics: FRODO in *Methods in Enzymology* (Carter Jr., C.W. and Sweet, R.W., eds.) Vol. 115, pp. 157–171, Academic Press, New York
35. Brunger, A.T. (1987) *A System for X-Ray Crystallography and NMR, X-PLOR Manual-Version 3.1*, Yale University Press, New Haven and London
36. Brunger, A.T., Adams, P.D., Clore, G.M., Delano, W.L., Gros, P., Grosse-Kunstleve, R.W., Jiang, J.S., Kuszewski, J., Nilges, M., Pannu, N.S., Read, R.J., Rice, L.M., Simonson, T., and Warren, G.L. (1998) Crystallography & NMR system: A new software suite for macromolecular structure determination. *Acta Cryst.* **D54**, 905–921
37. Jiang, J.-S. and Brünger, A.T. (1994) Protein hydration observed by X-ray diffraction: solvation properties of penicillopepsin and neuraminidase crystal structures. *J. Mol. Biol.* **243**, 100–115
38. Kraulis, P.J. (1991) MOLSCRIPT: a program to produce both detailed and schematic plots of protein structures. *J. Appl. Cryst.* **24**, 946–950

39. Jones, T.A., Zou, J.Y., Cowan, S.W., and Kjeldgaard, M. (1991) Improved methods for binding protein models in electron density maps and the location of errors in these models. *Acta Cryst.* **A47**, 110–119
40. Kauzmann, W. (1959) Some factors in the interpretation of protein denaturation. *Adv. Protein Chem.* **14**, 1–63
41. Takano, K., Yamagata, Y., and Yutani, K. (1998) A general rule for the relationship between hydrophobic effect and conformational stability of a protein: Stability and structure of a series of hydrophobic mutants of human lysozyme. *J. Mol. Biol.* **280**, 749–761
42. Funahashi, J., Takano, K., Yamagata, Y., and Yutani, K. (1999) Contribution of amino acid substitutions at two different interior positions to the conformational stability of human lysozyme. *Protein Eng.* **12**, 841–850
43. Connolly, M.L. (1993) The molecular surface package. *J. Mol. Graph.* **11**, 139–141
44. Ota, M., Kanaya, S., and Nishikawa, K. (1995) Desk-top analysis of the structural stability of various point mutations introduced into ribonuclease H. *J. Mol. Biol.* **248**, 733–738
45. Takano, K., Ota, M., Ogasahara, K., Yamagata, Y., Nishikawa, K., and Yutani, K. (1999) Experimental verification of the "stability profile of mutant protein" (SPMP) data using mutant human lysozymes. *Protein Eng.* **12**, 663–672
46. Pappenberger, G., Schurig, H., and Jaenicke, R. (1997) Disruption of an ionic network leads to accelerated thermal denaturation of D-glyceraldehyde-3-phosphate dehydrogenase. *J. Mol. Biol.* **274**, 676–683
47. Barlow, D.J. and Thornton, J.M. (1983) Ion-pairs in proteins. *J. Mol. Biol.* **168**, 867–885
48. Takano, K., Yamagata, Y., Funahashi, J., Hioki, Y., Kuramitsu, S., and Yutani, K. (1999) Contribution of intra- and intermolecular hydrogen bonds to the conformational stability of human lysozyme. *Biochemistry* **38**, 12698–12708
49. Oobatake, M. and Ooi, T. (1993) Hydration and heat stability effects on protein unfolding. *Prog. Biophys. Mol. Biol.* **59**, 237–284
50. Eriksson, A.E., Baase, W.A., Zhang, X.-J., Heinz, D.W., Blaber, M., Baldwin, E.P., and Matthews, B.W. (1992) Response of a protein structure to cavity-creating mutations and its relation to the hydrophobic effect. *Science* **255**, 178–183
51. Funahashi, J., Takano, K., and Yutani, K. (2001) Are the parameters of various stabilization factors estimated from mutant human lysozymes compatible with other proteins? *Protein Eng.* **14**, 127–134